WILEY-VCH

RESEARCH ARTICLE

Bimetallic Single Atom/Nanoparticle Ensemble for Efficient Photochemical Cascade Synthesis of Ethylene from Methane

Yin-Feng Wang,[a] Ming-Yu Qi,[b] Marco Conte,[c] Zi-Rong Tang,*[a] and Yi-Jun Xu*[a]

[a] Y.-F. Wang, Prof. Dr. Z.-R. Tang, Prof. Dr. Y.-J. Xu
College of Chemistry, State Key Laboratory of Photocatalysis on Energy and Environment, Fuzhou University
Fuzhou 350116 (China)
E-mail: zrtang@fzu.edu.cn; yjxu@fzu.edu.cn
Homepage: http://xugroup.fzu.edu.cn
[b] Dr. M.-Y. Qi
Institute of Fundamental and Frontier Sciences, University of Electronic Science and Technology of China
Chengdu 611731 (China)
[c] Dr. M. Conte
Department of Chemistry, University of Sheffield, Sheffield, S3 7HF, (UK)

Supporting information for this article is given via a link at the end of the document.

Abstract: Light-driven photoredox catalysis presents a promising approach for the activation and conversion of methane (CH_4) into high value-added chemicals under ambient conditions. However, the high C−H bond dissociation energy of CH_4 and the absence of well-defined C−H activation sites on catalysts significantly limit the highly efficient conversion of CH_4 toward multicarbon (C_{2+}) hydrocarbons, particularly ethylene (C_2H_4). Herein, we demonstrate a bimetallic design of Ag nanoparticles (NPs) and Pd single atoms (SAs) on ZnO for the cascade conversion of CH_4 into C_2H_4 with the highest production rate compared with previous works. Mechanistic studies reveal that the synergistic effect of Ag NPs and Pd SAs, upon effecting key bond-breaking and -forming events, lowers the overall energy barrier of the activation process of both CH_4 and the resulting C_2H_6, constituting a truly synergistic catalytic system to facilitate the C_2H_4 generation. This work offers a novel perspective on the advancement of photocatalytic directional CH_4 conversion toward high value-added C_{2+} hydrocarbons through the subtle design of bimetallic cascade catalyst strategy.

Introduction

Methane (CH_4), the main component of natural gas and shale gas, is considered one of the most promising chemical feedstocks due to its high abundance and relatively low cost in the context of dwindling petroleum reserves.[1] Upgrading CH_4 into high value-added chemicals via nonoxidative or oxidative pathways is a win-win strategy that maximizes the value of CH_4 for clean energy development and reduces carbon footprint.[2] Nonoxidative coupling of methane (NOCM) has emerged as an attractive approach for CH_4 conversion, where CH_4 is directly converted to multicarbon (C_{2+}) compounds through C−H activation without any oxidant intervention, thus avoiding the overoxidation of CH_4 that results in undesired carbon oxides.[3] However, owing to the low polarizability and high C−H bonding energy of CH_4, NOCM requires extremely high temperatures, typically leading to severe coke deposition and catalyst deactivation.[4] Under such circumstances, light-driven photoredox catalysis is seen as a prospective alternative for NOCM on account of its ability to overcome thermodynamic limitations by providing photon energy as a driving force to enable NOCM to occur under ambient conditions.[5]

Among the products of photocatalytic NOCM, ethylene (C_2H_4), one of the most widely used feedstocks in the chemical industry, is of considerable importance due to its high energy content and market price. To date, however, the C_{2+} compounds generated by photocatalytic NOCM are predominantly ethane (C_2H_6) rather than the more valuable C_2H_4.[6] From the perspective of the reaction mechanism, the conversion of CH_4 to C_2H_4 is a tandem process involving the C−C coupling of CH_4 and the dehydrogenation of the resulting C_2H_6 intermediate.[7] This multistep conversion includes a variety of intermediates, such as methyl (CH_3) species, C_2H_6, ethyl (C_2H_5) species, to name a few,[8] whose adsorption and desorption behavior on the catalyst strongly influence the distribution of the end products. Notably, the grand challenge in the CH_4 conversion to C_2H_4 is the gas-phase dehydrogenation of C_2H_6 under mild conditions,[7a] which requires a catalyst with active sites for the simultaneous activation of both reactant CH_4 and intermediate C_2H_6. In such a scenario, synergistic catalysis is expected to be a potential strategy to overcome the current bottleneck limitation of CH_4-to-C_2H_4 transformation in view of the judicious combination of designed multifunctional active sites, spatially distributed on the catalyst surface, could sequentially promote chemical reactions that cannot be accessibly catalyzed by a single active site.[9]

Herein, we developed a facile ball milling method to co-modify Ag nanoparticles (NPs) and Pd single atoms (SAs) on ZnO (a classical catalyst support commonly used for CH_4 conversion) for efficient photocatalytic CH_4 nonoxidative conversion toward C_2H_4 production under ambient conditions. Our methodology utilizes two synergistically working metal active sites, Ag and Pd, with complementary functions that significantly lower the overall energy barrier of the CH_4 conversion process while increasing catalytic activity, where each metal site plays a dominant role at different steps during the reaction. Comprehensive mechanistic studies reveal that Ag NPs are capable of facilitating the cleavage of the C−H bonds of both CH_4 and C_2H_6. Nevertheless, when CH_4 and C_2H_6 coexist, single Ag sites preferentially promote C_2H_6 activation, which is detrimental to the sustainable conversion of

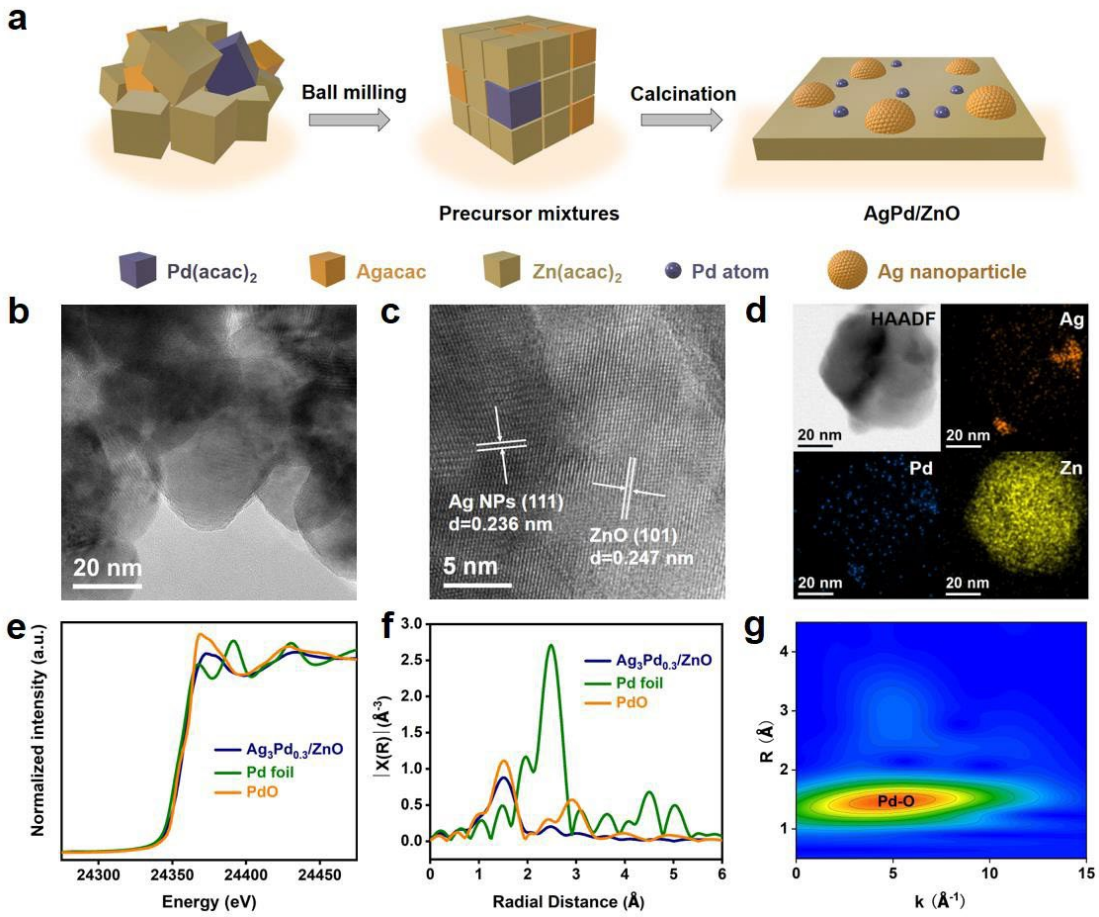

Figure 1. a) Schematic illustration for the synthesis of the AgPd/ZnO composites. b–c) TEM image and HRTEM image of $Ag_3Pd_{0.3}$/ZnO. d) HAADF-STEM image and the elemental mapping results of $Ag_3Pd_{0.3}$/ZnO. e–f) Normalized Pd K-edge XANES spectra and FT-EXAFS spectra of $Ag_3Pd_{0.3}$/ZnO in reference to Pd foil and PdO. g) Wavelet transform for Pd K-edge EXAFS spectra of $Ag_3Pd_{0.3}$/ZnO.

CH_4. In contrast, the features of Pd SAs selectively promote the C−H activation of CH_4, thus enhancing the efficiency of CH_4 conversion. This work reveals the mechanism of bimetallic synergistic catalysis of CH_4 conversion, providing a new reference for CH_4 conversion to C_2H_4 by ingeniously designing photocatalytic cascade systems with well-defined sites.

Results and Discussion

The schematic of the overall fabrication procedure of Ag and Pd co-modified ZnO (AgPd/ZnO) bimetallic catalysts is shown in **Figure 1a**. Specifically, corresponding metal precursors are simultaneously added to an agate jar for mechanical mixing. After calcination, the AgPd/ZnO composites are obtained, and the resulting sample is denoted as Ag_xPd_y/ZnO, where x and y represent the mass percentage of Ag and Pd, respectively. The method is capable of precisely controlling the Pd and Ag content by adjusting the amount of Pd and Ag precursors (**Table S1**). As observed from the transmission electron microscopy (TEM) images (**Figure 1b** and **Figure S1**), Ag-derived nanoparticles (NPs) with particle size greater than 10 nm are randomly distributed on the surface of ZnO NPs. Since the catalysts are synthesized by ball milling, the morphology of Ag species and ZnO is inevitably irregular nanoparticle.[10] In addition, the formation of Pd-derived nanoparticles is not observed because the content of Pd is too low.[11] In the obtained high-resolution transmission electron microscopy (HRTEM) images, the two well-defined lattice fringes with d-spacing of 0.236 and 0.247 nm correspond to the (111) plane of Ag NPs and the (101) crystal plane of ZnO, respectively (**Figure 1c**).[12] High-angle annular dark-field scanning TEM (HAADF-STEM) images and elemental mapping confirm the presence of Zn, O, Ag, and Pd elements in $Ag_3Pd_{0.3}$/ZnO (**Figure 1d**). X-ray photoelectron spectroscopy (XPS) was carried out to further analyze the chemical elemental composition and valence states of samples (**Figure S2**). The coexistence of the elements Ag, Pd, Zn and O of $Ag_3Pd_{0.3}$/ZnO in the survey XPS spectrum is consistent with the aforementioned elemental mapping results. Furthermore, the XPS results demonstrate the existence of metallic Ag and Pd^{2+} in $Ag_3Pd_{0.3}$/ZnO. The crystalline phase of samples was investigated by X-ray diffraction (XRD) as displayed in **Figure S3**. All samples exhibit the typical peaks attributed to hexagonal wurtzite ZnO (PDF#36-1451). A weak additional diffraction peak appears at 38° in all Ag-containing samples, which is indexed to the (111) plane of Ag NPs (PDF#04-0783).[13] However, no Pd-derived diffraction peak is observed in $Ag_3Pd_{0.3}$/ZnO, probably owing to the low content or high dispersion on ZnO.[14] The light absorption property of samples was determined by ultraviolet-visible (UV/Vis) diffuse reflectance spectroscopy (DRS) in **Figure S4**. The absorption edge of pristine ZnO in the ultraviolet band is ca. 380 nm, which corresponds to the intrinsic bandgap (3.2 eV) absorption of ZnO. A significantly enhanced light absorption is observed in the visible light region after the introduction of

10.1002/anie.202407791

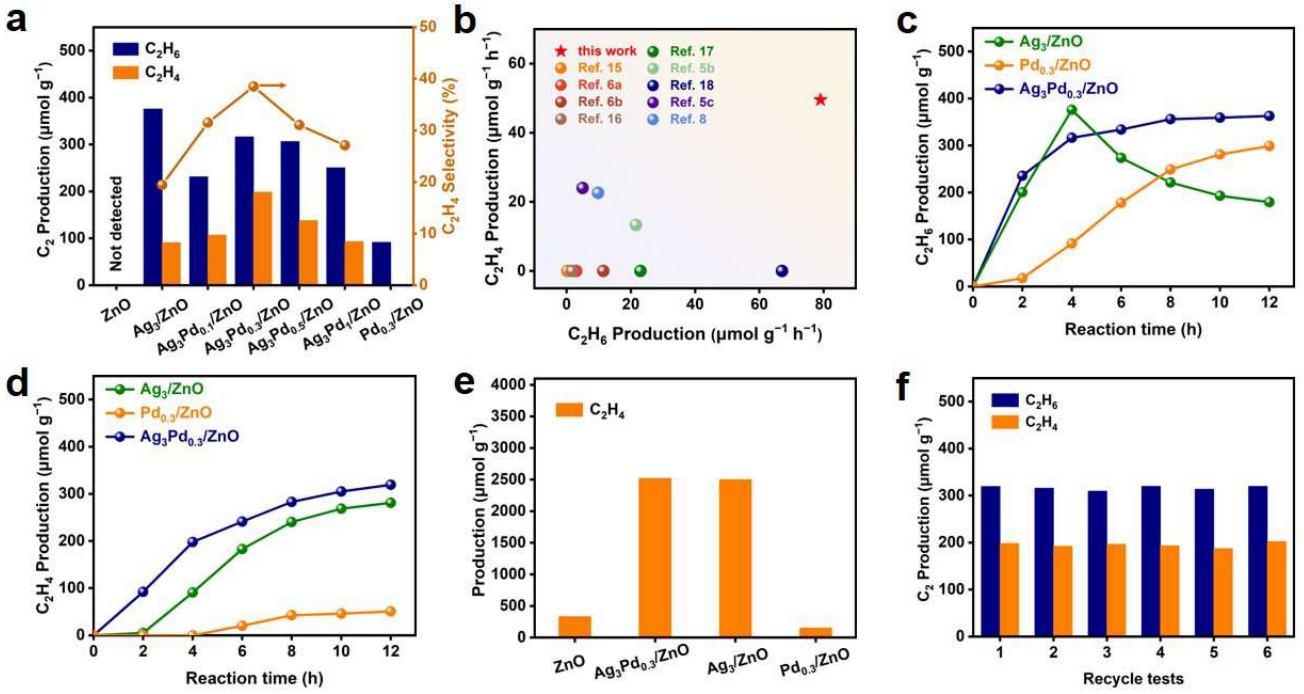

Figure 2. a) Photocatalytic CH_4 conversion performance of various catalysts after 4 h of illumination. b) The performance summary of the CH_4 nonoxidative conversion to C_2 compound in this work and other representative reported photocatalysts (Ga_2O_3-K[15], (Zn^+,Zn^{2+})-ZSM-5[6a], Au/m-ZnO[6b], Nb-TiO_2-SiO_2[16], Ag-HPW/TiO_2[17], ZnO-AuPd[5b], Pt/Ga_2O_3[18], $Pd_5/Zn_{0.35}$-WO_3[5c], Au_2-Pd_2/BNOF[8]). The detailed reaction condition of these representative works is presented in **Table S3**. c) Time-dependent photocatalytic C_2H_6 production over Ag_3/ZnO, $Pd_{0.3}$/ZnO and $Ag_3Pd_{0.3}$/ZnO. d) Time-dependent photocatalytic C_2H_4 production over Ag_3/ZnO, $Pd_{0.3}$/ZnO and $Ag_3Pd_{0.3}$/ZnO. e) Photocatalytic C_2H_6 conversion performance of various catalysts after 4 h of illumination. f) C_2 compound yields in the recycle tests of $Ag_3Pd_{0.3}$/ZnO (each cycle lasts 4 h).

Ag and Pd, which is due to their interband absorption or scattering.[19]

The coordination environment of Pd in $Ag_3Pd_{0.3}$/ZnO was further investigated by synchrotron-based X-ray absorption fine structure (XAFS) spectroscopy. The Pd K-edge XANES spectra of $Ag_3Pd_{0.3}$/ZnO show its threshold energy (E_0) and white-line peak close to standard PdO, indicating that the electronic state of Pd in $Ag_3Pd_{0.3}$/ZnO is +2 (**Figure 1e**).[11] In **Figure 1f** and **g**, the extended X-ray adsorption fine structure (EXAFS) spectra of Pd K-edge in R-space and wavelet transformations of the Pd K-edge EXAFS spectra exhibit only a single-peak signal of Pd−O coordination on $Ag_3Pd_{0.3}$/ZnO, confirming that Pd is dispersed as isolated single atoms and coordinated with O atoms in the $Ag_3Pd_{0.3}$/ZnO.[20] The quantitative coordination configuration of individual Pd atoms is derived based on EXAFS curve fitting, and the average coordination number (CN) of Pd−O in $Ag_3Pd_{0.3}$/ZnO is determined to be 4 ± 0.2 (**Figure S5** and **Table S2**).[21]

Upon confirming the structural information of the prepared samples, we evaluated their performance for photocatalytic CH_4 conversion in the gas-solid phase (1 mL CH_4 in argon (Ar), 1 atm pressure) under Xe lamp illumination. As displayed in **Figure 2a**, no C_2 compounds are detected over pristine ZnO. After the modification of Ag, the yield of C_2 compounds was significantly improved (**Figure S6**). In particular, the optimized Ag_3/ZnO shows excellent photocatalytic CH_4 conversion performance (376 μmol g^{-1} of C_2H_6 and 90.8 μmol g^{-1} of C_2H_4 after 4 h of light irradiation). Considering the feature of Pd in the breakage of the C−H bond of CH_4,[22] Pd was introduced into Ag_3/ZnO to further enhance the CH_4 conversion performance (**Figure S7**). After optimizing the Pd loading amount, $Ag_3Pd_{0.3}$/ZnO exhibits the optimal catalytic performance (515 μmol g^{-1} of C_2 compounds with C_2H_4 selectivity of 39% under 4 h of illumination), which is superior to most of the recent works on CH_4 conversion to C_2 compounds (**Figure 2b** and **Table S3**). The C_2H_4 yield of $Ag_3Pd_{0.3}$/ZnO is more than double that of Ag_3/ZnO, whereas only a small amount of C_2H_6 is detected on $Pd_{0.3}$/ZnO during the same reaction time. These results clearly demonstrate the importance of the synergistic effect of Ag and Pd in promoting the conversion of CH_4 to C_2H_4.

A series of blank experiments have been carried out, which show that no C_2 products could be detected in the absence of photocatalyst, under dark conditions, or without CH_4, demonstrating that this is a photocatalytic process and CH_4 is the only carbon source (**Figure S8a**). Isotopic labeling tests using $^{13}CH_4$ as the feedstock further confirm the origin of the resulting C_2H_4 and C_2H_6. As shown in **Figure S8b**, dominant peaks attributed to $^{13}C_2H_4$ and $^{13}C_2H_6$ and their molecular fragments can be observed, such as $^{13}C_2H_4$ (m/z=30, 29, 28) and $^{13}C_2H_6$ (m/z=32, 31, 30, 29, 28), respectively.[14] These results collectively indicate that the generated C_2 compounds undoubtedly originate from the feedstock CH_4.

To evaluate the long-term stability of the photocatalysts, we further performed time-dependent measurements with continuous light irradiation for 12 h over prepared samples. As shown in **Figure S9**, the C_2H_6 yield of $Ag_3Pd_{0.3}$/ZnO gradually increases and then becomes steady along with the duration of illumination time, while the yield and selectivity of C_2H_4 enhance continuously.

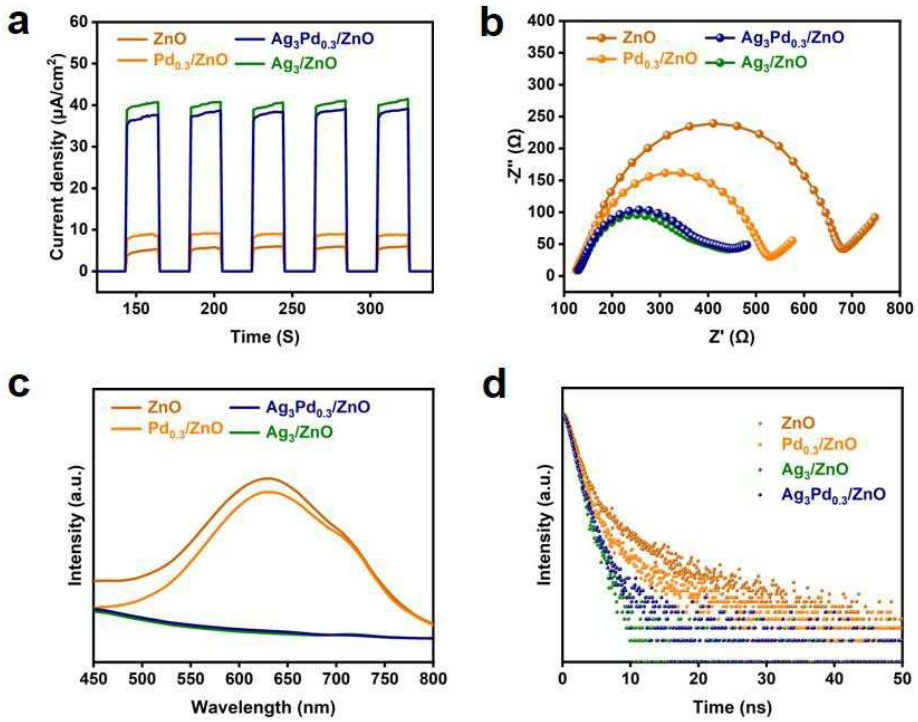

Figure 3. a) Transient photocurrent spectra, b) EIS spectra, c) steady-state PL emission spectra and d) TRPL spectra of various catalysts.

Specifically, $Ag_3Pd_{0.3}$/ZnO achieves a yield of 682 μmol g^{-1} of the C_2 compounds after 12 h of reaction (47% selectivity for C_2H_4). Interestingly, in the case of Ag_3/ZnO, the generated C_2H_6 is consumed with the extension of reaction time and at a rate comparable to the rate of increase of C_2H_4 (**Figure 2c** and **d**), implying that C_2H_4 is converted from the generated C_2H_6. This illustrates that Ag NPs not only facilitate the C−H activation of CH_4, but also supply active sites for the conversion of C_2H_6 to C_2H_4. On the other hand, Ag NPs alone preferentially accelerate the activation of C_2H_6 when CH_4 and C_2H_6 coexist, which is detrimental to the sustainable conversion of CH_4, also demonstrating the limited functionality of a single active site. Apparently, the features of Pd SAs in promoting the CH_4 activation compensate for this drawback in our system. Besides, we also implement comparative experiments using C_2H_6 as feedstock (**Figure 2e**, 1 mL C_2H_6 in Ar, 1 atm pressure). As expected, both $Ag_3Pd_{0.3}$/ZnO and Ag_3/ZnO lead to superior C_2H_6 conversion performance (2500 μmol g^{-1} of C_2H_4 with C_2H_4 selectivity of ~100% under 4 h of illumination). In contrast, C_2H_4 production on pristine ZnO and $Pd_{0.3}$/ZnO is almost negligible, further demonstrating the excellent performance of Ag NPs for the efficient and selective conversion of C_2H_6 to C_2H_4. It should be noted that the stoichiometric mismatch between the H_2 evolution and the yield of C_2 compounds is closely related to the consumption of lattice oxygen in ZnO during the reaction (**Figure S10**).[5b, 23] The lattice oxygen consumed in ZnO can be regenerated by heating the catalyst in air to restore its catalytic activity. Durability measurements show that $Ag_3Pd_{0.3}$/ZnO maintains good catalytic performance during six cycling tests, with each cycle lasting 4 h (**Figure 2f**). Additionally, the leaching of Ag and Pd during the cycling test is negligible according to the ICP-AES results (**Table S4**). As such, a durable photochemical CH_4 conversion can be achieved by recovering and reusing the catalyst.

Photoelectrochemical and photoluminescence (PL) characterization were further performed to reveal the effect of photogenerated charge separation/transfer on photocatalytic CH_4 conversion performance.[24] The transient photocurrent response and electrochemical impedance spectroscopy (EIS) spectra show that the modification of Ag significantly improves the photogenerated charge separation efficiency (**Figure 3a** and **b**). However, the similar photoelectrochemical properties of Ag_3/ZnO and $Ag_3Pd_{0.3}$/ZnO indicate that the introduction of Pd SAs does not further promote charge separation efficiency. As presented in **Figure 3c** and **d**, PL and time-resolved PL (TRPL) characterization results also show a similar tendency, implying that the effect of Pd SAs on the suppression of electron-hole pairs recombination is extremely limited compared to Ag NPs (**Table S5**). The inconsistency between the photoelectric efficiency and photocatalytic performance for CH_4 conversion implies that the separation and transfer of photogenerated charge carriers are not the dominant factors affecting the C_2H_4 production in our system.

It is well known that the photocatalytic CH_4 conversion process involves light absorption, photogenerated charge carrier separation/transfer, and interaction between the catalyst active sites and the CH_4 molecule.[1d, 25] The above characterization results indicate that the former two stages do not have a decisive influence on C_2H_4 production. In order to gain insight into the functional orientation of catalyst surface sites during CH_4 conversion, the CH_4 adsorption experiment on the samples was first performed by CH_4 temperature-programmed-desorption (TPD) analysis. As shown in **Figure 4a**, the desorption peak at

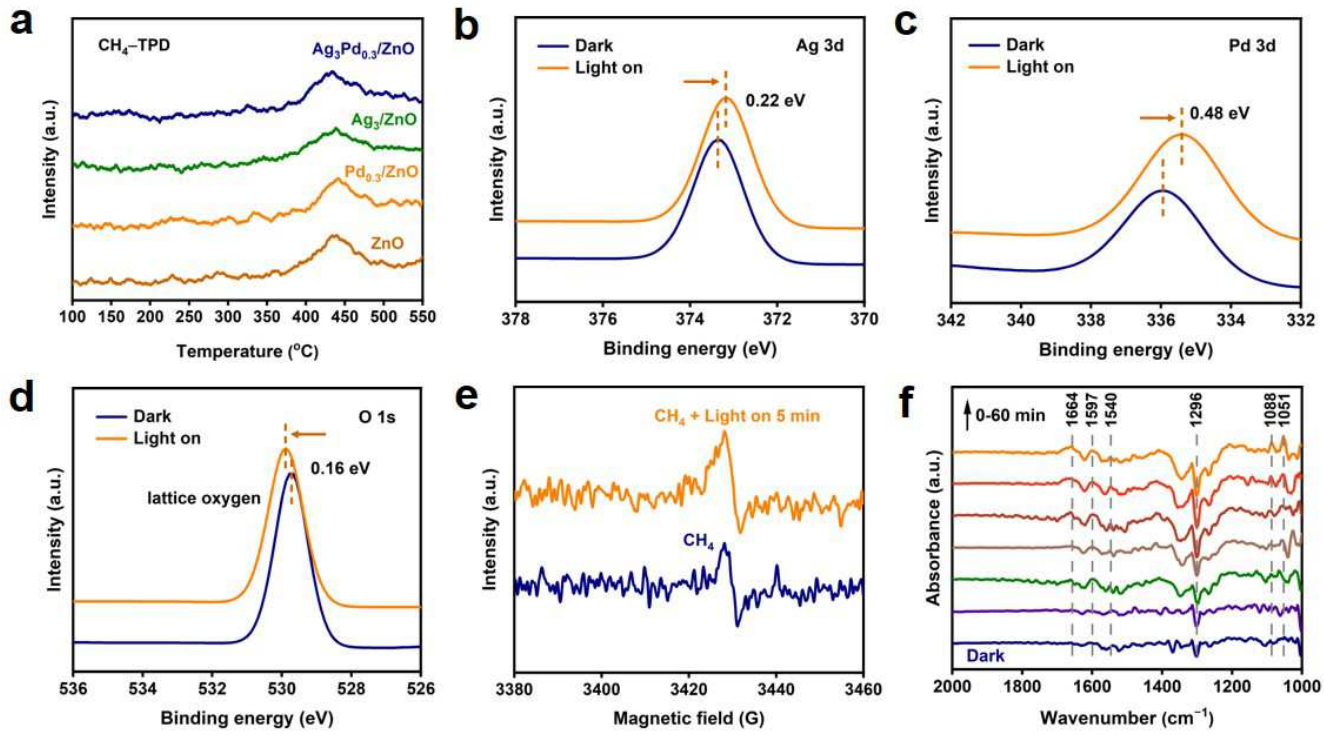

Figure 4. a) CH_4-TPD profiles of various catalysts. b) In situ Ag 3d XPS spectra of $Ag_3Pd_{0.3}$/ZnO under the dark condition and light irradiation. c) In situ Pd 3d XPS spectra of Ag_3Pd_1/ZnO under the dark condition and light irradiation. d) In situ O 1s XPS spectra of $Ag_3Pd_{0.3}$/ZnO under the dark condition and light irradiation. e) In situ EPR signals of $Ag_3Pd_{0.3}$/ZnO collected in CH_4 atmosphere. f) In situ DRIFTS spectra for photocatalytic conversion of CH_4 over $Ag_3Pd_{0.3}$/ZnO.

around 440 °C is attributed to the strong adsorption of CH_4 on the catalyst surface.[26] The modification of Ag and Pd hardly affects the adsorption behavior of CH_4 on ZnO surface. In situ XPS was performed to further explore the carrier transfer behavior (**Figure 4b-d** and **Figure S11**). During light irradiation, a negative shift of ~0.22 eV of the Ag 3d peak can be clearly observed, suggesting that Ag works as an electron acceptor during the reaction. However, it is difficult to recognize the clear signal of Pd 3d of $Ag_3Pd_{0.3}$/ZnO due to the low weight content. Therefore, Ag_3Pd_1/ZnO with higher Pd content prepared under the same conditions was used to investigate the function of Pd. The negative shift of ~0.48 eV of Pd 3d peak under illumination implies that Pd also acts as an electron acceptor in the reaction. In parallel, O 1s peak exhibits a positive shift of 0.16 eV, indicating that holes are aggregated at the oxygen sites of ZnO for CH_4 activation.[27] In situ electron paramagnetic resonance (EPR) measurements for the oxygen vacancies of the samples further support this conclusion (**Figure 4e** and **Figure S12a**). The signal intensity of oxygen vacancies on $Ag_3Pd_{0.3}$/ZnO is enhanced under the CH_4 atmosphere upon illumination, whereas no significant signal change is observed on pristine ZnO, demonstrating that the lattice oxygen sites enriched by photogenerated holes are consumed during the reaction.

In situ Fourier transform infrared spectroscopy (FT-IR) method was employed to further detect CH_4 intermediates during the reaction. In **Figure 4f**, a new peak around 1540 cm^{-1} attributed to the C−H symmetry vibration of adsorbed CH_4 and the decrease of the peak around 1296 cm^{-1} belonging to free CH_4 molecules collectively demonstrate the photoenhanced CH_4 adsorption, which is induced by the photogenerated Zn^+−O^- pairs on the ZnO surface.[28] Simultaneously, the peak at 1664 cm^{-1} is assigned to the surface-adsorbed hydroxyl species associated with the surface lattice oxygen of ZnO adsorbing the cleaved H atoms extracted from CH_4.[29] Furthermore, the peak around 1597 cm^{-1} is ascribed to the bending vibration of the O−H bond of H_2O molecules,[30] suggesting that H_2O is generated during the CH_4 conversion reaction, which is the destination of the lattice oxygen consumed in ZnO and the H atoms adsorbed on these lattice oxygen as mentioned in the previous section. Notably, the peaks located at 1051 cm^{-1} and 1088 cm^{-1} are attributed to the surface-adsorbed ethyl (C_2H_5*) and methyl (CH_3*) species, which are key intermediates for the formation of C_2H_4 and C_2H_6, respectively.[5b, 8] In sharp contrast, the signals of these CH_4-derived intermediates are not detected on ZnO (**Figure S13a**), meaning that the CH_4 to C_2H_4 conversion reaction cannot proceed without Ag NPs and Pd SAs although the photogenerated Zn^+−O^- sites on substrate ZnO can trigger CH_4 activation. Taken together, the interactions between CH_4-derived intermediates and metal sites (Ag NPs and Pd SAs) are significant for CH_4 conversion.

To gain insights into the nature of the active sites on the catalyst surface for the conversion of CH_4 to C_2H_4, density-functional theory (DFT) calculations of the reaction mechanism were performed. Two models are built and optimized to simulate the structures of pristine ZnO and AgPd/ZnO (**Figure S14**). As depicted in **Figure S15**, the first deprotonation step of CH_4 over pristine ZnO is endergonic by the activation energy of 0.72 eV,

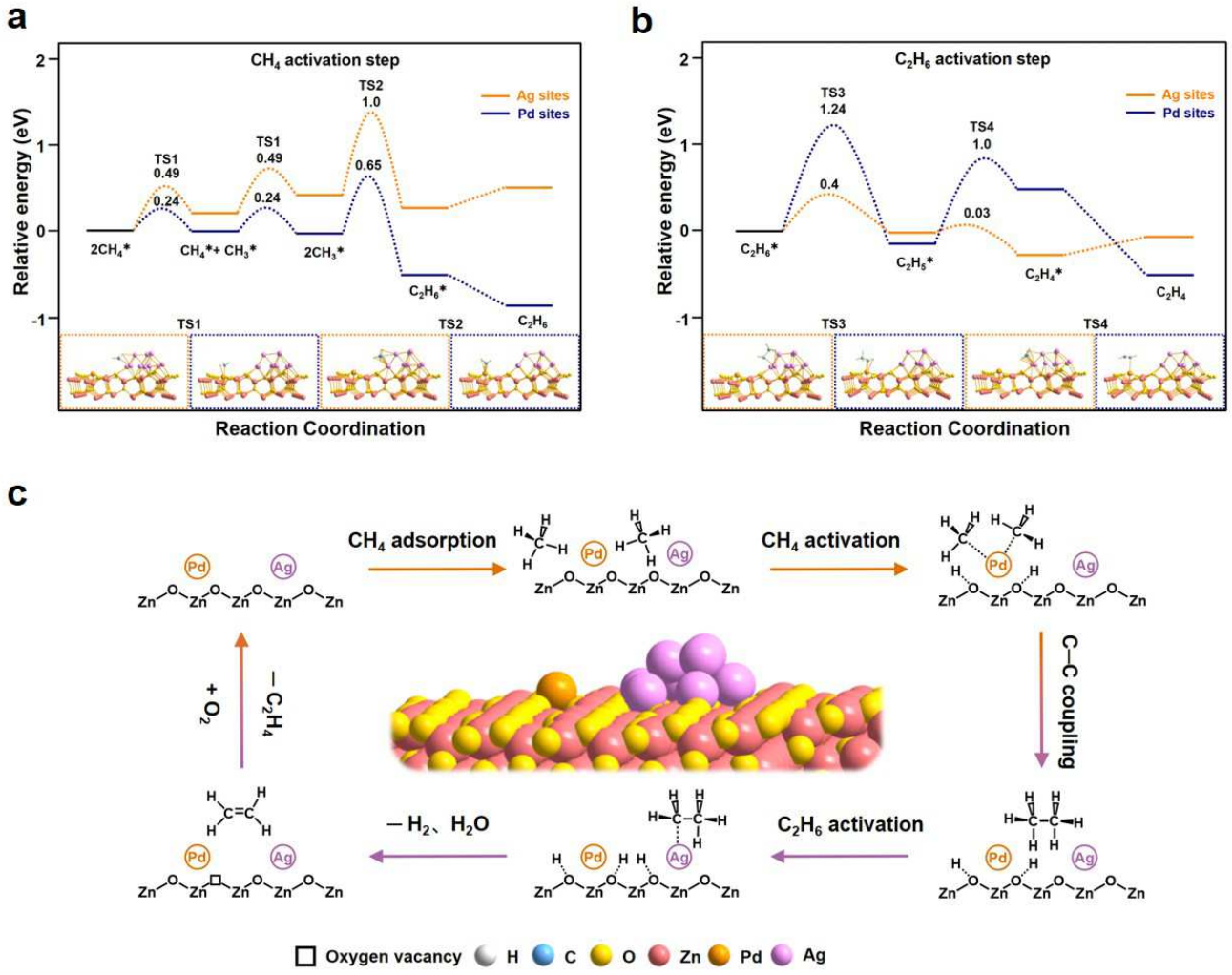

Figure 5. Calculated potential energy diagrams for a) the CH_4 activation step and b) the C_2H_6 intermediate activation step in the CH_4 conversion to C_2H_4 at Ag sites and Pd sites on AgPd/ZnO. c) Schematic illustration for photocatalytic CH_4 nonoxidative conversion toward C_2H_4 over AgPd/ZnO. Insets: atomic configurations of the reaction intermediates.

dissociating into CH_3*. Due to the high energy barrier (5.7 eV), the thermodynamic infeasibility of the C−C coupling of CH_3* hinders the progress of the reaction. Such a high energy barrier of C−C coupling is attributed to the strong adsorption of CH_3* on the lattice oxygen of ZnO (−3.27 eV, **Table S6**). In **Figure 5a**, with the introduction of Ag NPs and Pd SAs, the C−H dissociation energy of CH_4 is significantly decreased to an energy barrier of 0.49 eV and 0.24 eV, respectively, thus effectively promoting the C-H bond activation of CH_4. Thereafter, the C−C coupling of CH_3* over Ag and Pd sites only requires overcoming energy barriers of 1 eV and 0.65 eV, respectively. Obviously, Ag NPs and Pd SAs are more conducive to the generation of C_2H_6 owing to the weak interaction between CH_3* and the metal sites (0.36 eV at Ag sites and −0.06 eV at Pd sites, **Table S7**). As the reaction further proceeded, the generated C_2H_6 undergoes another dehydrogenation process to form C_2H_4 (**Figure 5b**). Similar to the activation process of CH_4, Ag sites accelerate the deprotonation of C_2H_6 by overcoming a moderate energy barrier of 0.4 eV to form C_2H_5*, which is subsequently dehydrogenated to C_2H_4. Notably, DFT calculations show that Ag sites are more thermodynamically capable of promoting C_2H_6 activation than CH_4 activation, consistent with the experimental results. In contrast, the C_2H_6 activation is significantly harder thermodynamically at the Pd sites due to the high energy barrier of 1.24 eV. As a consequence of this as well as the low desorption energy of C_2H_6 at the Pd sites (−0.35 eV, **Table S7**), the C_2H_6 generated at the Pd sites is desorbed into the gas phase followed by adsorption and dehydrogenation at the Ag sites.

Based on the above experimental and theoretical results, the overall catalytic reaction mechanism is proposed (**Figure 5c**). Initially, photogenerated charge carriers are generated on ZnO upon light illumination. The photogenerated holes enriched in the lattice oxygen sites of ZnO, activating the C−H bond cleavage of CH_4 to form CH_3*. Subsequently, C−C coupling of CH_3* occurs on Pd SAs to generate C_2H_6. Finally, the generated C_2H_6 deprotonates to C_2H_5*, which migrates to the Ag sites for dehydrogenation to C_2H_4. Meanwhile, some of the H atoms extracted from CH_4 are reduced to H_2 by photogenerated electrons, and the remaining H atoms combine with the lattice oxygen of ZnO to form H_2O.

Conclusion

In summary, we present a bimetallic synergistic catalytic strategy for the cascade photocatalytic CH_4 conversion to C_2H_4 over ZnO co-modified with Ag NPs and Pd SAs. Our system demonstrates superior performance in photocatalytic nonoxidative coupling of CH_4 to C_2H_4, providing a high CH_4 conversion of 1.4 mmol g^{-1} with a high C_2H_4 selectivity of nearly 50% after 12 h of illumination, which is greatly superior to most of the recent works on NOCM. Mechanistic studies show that Ag NPs and Pd SAs on ZnO acting as electron acceptors during the reaction effectively promote the separation/transfer of photogenerated charge carriers. More importantly, Pd SAs and Ag NPs synergistically contribute to the generation of C_2H_4 by promoting the C−H activation of both CH_4 and the resulting C_2H_6, respectively. This work highlights the key importance of the sensible design of well-defined catalyst with functionally complementary multiple active sites as an appealing strategy for the sustainable and directional conversion of CH_4 to high value-added hydrocarbons.

Acknowledgements

This work was supported by the Natural Science Foundation of China (22172030, 22072023, 21872029, U1463204, and 21173045), the Program for National Science and Technology Innovation Leading Talents (00387072), the Program for Leading Talents of Fujian Universities, the 1st Program of Fujian Province for Top Creative Young Talents, the China Postdoctoral Science Foundation (2023M740513), the Jiangxi Province “Double Thousand Plan” (No. jxsq2023102143), and the Natural Science Foundation of Fujian Province (2017J07002 and 2019J01631).

Keywords: photocatalysis, methane conversion, C−H activation, ethylene, bimetallic sites

[1] a) S. J. Xie, W. C. Ma, X. J. Wu, H. K. Zhang, Q. H. Zhang, Y. D. Wang, Y. Wang, *Energy Environ. Sci.* **2021**, *14*, 37-89; b) P. Schwach, X. L. Pan, X. H. Bao, *Chem. Rev.* **2017**, *117*, 8497-8520; c) N. F. Dummer, D. J. Willock, Q. He, M. J. Howard, R. J. Lewis, G. D. Qi, S. H. Taylor, J. Xu, D. Bethell, C. J. Kiely, G. J. Hutchings, *Chem. Rev.* **2023**, *123*, 6359-6411; d) D. Hu, V. V. Ordomsky, A. Y. Khodakov, *Appl. Catal., B* **2021**, *286*, 119913; e) Y.-H. Jiang, S.-Y. Li, Y.-Y. Fan, Z.-Y. Tang, *Angew. Chem., Int. Ed.* **2024**, e202404658.

[2] a) Q. Li, Y.-X. Ouyang, H.-L. Li, L.-B. Wang, J. Zeng, *Angew. Chem., Int. Ed.* **2022**, *61*, e202108069; b) M. Ravi, M. Ranocchiari, J. A. van Bokhoven, *Angew. Chem., Int. Ed.* **2017**, *56*, 16464-16483; c) N. J. Gunsalus, A. Koppaka, S. H. Park, S. M. Bischof, B. G. Hashiguchi, R. A. Periana, *Chem. Rev.* **2017**, *117*, 8521-8573.

[3] a) X. G. Meng, X. J. Cui, N. P. Rajan, L. Yu, D. H. Deng, X. H. Bao, *Chem* **2019**, *5*, 2296-2325; b) H. Song, X. G. Meng, Z. J. Wang, H. M. Liu, J. H. Ye, *Joule* **2019**, *3*, 1606-1636.

[4] a) S.-Q. Wu, L.-Z. Wang, J.-L. Zhang, *J. Photochem. Photobiol., C* **2021**, *46*, 100400; b) S. Zhang, Q. Pessemesse, Z. J. Berkson, A. Van Bavel, A. D. Horton, P. A. Payard, C. Copéret, *Angew. Chem., Int. Ed.* **2023**, *62*, e202307814.

[5] a) X.-Y. Li, C. Wang, J.-W. Tang, *Nat. Rev. Mater.* **2022**, *7*, 617-632; b) W.-B. Jiang, J.-X. Low, K.-K. Mao, D.-L. Duan, S.-M. Chen, W. Liu, C.-W. Pao, J. Ma, S.-K. Sang, C. Shu, X.-Y. Zhan, Z.-m. Qi, H. Zhang, Z. Liu, X.-J. Wu, R. Long, L. Song, Y. J. Xiong, *J. Am. Chem. Soc.* **2021**, *143*, 269-278; c) Y.-D. Liu, Y.-H. Chen, W.-B. Jiang, T.-T. Kong, P. H. C. Camargo, C. Gao, Y. J. Xiong, *Research* **2022**, *2022*; d) Q. Y. Zhan, Y. X. Kong, X. H. Wang, L. Li, *Chem. Commun.* **2024**, *60*, 2732-2743; e) J. C. Colmenares, *Curr. Opin. Green Sustainable Chem.* **2019**, *15*, 38-46.

[6] a) L. Li, G.-D. Li, C. Yan, X.-Y. Mu, X.-L. Pan, X.-X. Zou, K.-X. Wang, J.-S. Chen, *Angew. Chem., Int. Ed.* **2011**, *50*, 8299-8303; b) L. Meng, Z. Chen, Z. Ma, S. He, Y. Hou, H.-H. Li, R. Yuan, X.-H. Huang, X. Wang, X. Wang, J. Long, *Energy Environ. Sci.* **2018**, *11*, 294-298.

[7] a) X.-G. Guo, G.-Z. Fang, G. Li, H. Ma, H.-J. Fan, L. Yu, C. Ma, X. Wu, D.-H. Deng, M.-M. Wei, D.-L. Tan, R. Si, S. Zhang, J. Q. Li, L.-T. Sun, Z.-C. Tang, X.-L. Pan, X.-H. Bao, *Science* **2014**, *344*, 616-619; b) J. H. Lunsford, *Catal. Today* **2000**, *63*, 165-174.

[8] C.-Y. Tang, S.-L. Du, H.-W. Huang, S.-Y. Tan, J.-W. Zhao, H.-W. Zhang, W.-K. Ni, X.-Y. Yue, Z.-X. Ding, Z.-Z. Zhang, R.-S. Yuan, W.-X. Dai, X.-Z. Fu, M. B. J. Roeffaers, J.-L. Long, *ACS Catal.* **2023**, *13*, 6683-6689.

[9] a) Y.-B. Huang, J. Liang, X.-S. Wang, R. Cao, *Chem. Soc. Rev.* **2017**, *46*, 126-157; b) D. E. Polyansky, D. C. Grills, M. Z. Ertem, K. T. Ngo, E. Fujita, *ACS Catal.* **2022**, *12*, 1706-1717.

[10] Y.-F. Hu, B.-L. Li, C.-L. Yu, H.-C. Fang, Z.-S. Li, *Mater. Today* **2023**, *63*, 288-312.

[11] M.-Y. Qi, M. Conte, Z.-R. Tang, Y.-J. Xu, *ACS Nano* **2022**, *16*, 17444-17453.

[12] F. Zhang, Y.-H. Li, M.-Y. Qi, Z.-R. Tang, Y.-J. Xu, *Appl. Catal., B* **2020**, *268*, 118380.

[13] Y.-S. Xie, N. Zhang, Z.-R. Tang, M. Anpo, Y.-J. Xu, *Catal. Today* **2020**, *340*, 121-127.

[14] X.-Y. Li, C. Wang, J.-L. Yang, Y.-X. Xu, Y. Yang, J.-G. Yu, J. J. Delgado, N. Martsinovich, X. Sun, X.-S. Zheng, W.-X. Huang, J.-W. Tang, *Nat. Commun.* **2023**, *14*, 6343.

[15] L. Yuliati, T. Hattori, H. Itoh, H. Yoshida, *J. Catal.* **2008**, *257*, 396-402.

[16] Z.-Y. Chen, S.-Q. Wu, J.-Y. Ma, S. Mine, T. Toyao, M. Matsuoka, L.-Z. Wang, J.-L. Zhang, *Angew. Chem., Int. Ed.* **2021**, *60*, 11901-11909.

[17] X. Yu, V. L. Zholobenko, S. Moldovan, D. Hu, D. Wu, V. V. Ordomsky, A. Y. Khodakov, *Nat. Energy* **2020**, *5*, 511-519.

[18] J.-Y. Ma, X.-J. Tan, Q.-Q. Zhang, Y. Wang, J.-L. Zhang, L.-Z. Wang, *ACS Catal.* **2021**, *11*, 3352-3360.

[19] S.-Y. Peng, L.-S. Yang, L.-S. Yu, X.-Y. Li, Y.-Z. Zhou, Y.-Y. Lv, F. Zhu, *New J. Chem.* **2019**, *43*, 18034-18040.

[20] P.-X. Liu, Y. Zhao, R.-X. Qin, S.-G. Mo, G.-X. Chen, L. Gu, D. M. Chevrier, P. Zhang, Q. Guo, D.-D. Zang, B.-H. Wu, G. Fu, N.-F. Zheng, *Science* **2016**, *352*, 797-801.

[21] Z. Chen, E. Vorobyeva, S. Mitchell, E. Fako, M. A. Ortuno, N. Lopez, S. M. Collins, P. A. Midgley, S. Richard, G. Vile, J. Perez-Ramirez, *Nat. Nanotechnol.* **2018**, *13*, 702-707.

[22] W.-Q. Zhang, C.-F. Fu, J.-X. Low, D.-L. Duan, J. Ma, W.-B. Jiang, Y.-H. Chen, H.-J. Liu, Z.-M. Qi, R. Long, Y.-F. Yao, X.-B. Li, H. Zhang, Z. Liu, J.-L. Yang, Z.-G. Zou, Y. J. Xiong, *Nat. Commun.* **2022**, *13*, 2806.

[23] a) X. Yu, V. De Waele, A. Lofberg, V. Ordomsky, A. Y. Khodakov, *Nat. Commun.* **2019**, *10*, 700; b) W.-Q. Zhang, D.-W. Xi, Y.-H. Chen, A. Chen, Y.-W. Jiang, H.-J. Liu, Z.-Y. Zhou, H. Zhang, Z. Liu, R. Long, Y. J. Xiong, *Nat. Commun.* **2023**, *14*, 3047.

[24] J.-Y. Li, C.-L. Tan, M.-Y. Qi, Z.-R. Tang, Y.-J. Xu, *Angew. Chem., Int. Ed.* **2023**, *62*, e202303054.

[25] M.-Y. Qi, M. Conte, M. Anpo, Z.-R. Tang, Y.-J. Xu, *Chem. Rev.* **2021**, *121*, 13051-13085.

[26] L. Fu, R.-X. Zhang, J.-L. Yang, J.-L. Shi, H.-Y. Jiang, J.-W. Tang, *Adv. Energy Mater.* **2023**, *13*, 2301118.

[27] P. Wang, R. Shi, Y.-X. Zhao, Z.-H. Li, J.-Q. Zhao, J.-Q. Zhao, G. I. N. Waterhouse, L.-Z. Wu, T.-R. Zhang, *Angew. Chem., Int. Ed.* **2023**, *62*, e202304301.

[28] a) X.-X. Chen, Y.-P. Li, X.-Y. Pan, D. Cortie, X.-T. Huang, Z.-G. Yi, *Nat. Commun.* **2016**, *7*, 12273; b) D. Scarano, S. Bertarione, G. Spoto, A. Zecchina, C. O. Areán, *Thin Solid Films* **2001**, *400*, 50-55.

[29] W. Wang, C.-Y. Deng, S.-J. Xie, Y.-F. Li, W.-Y. Zhang, H. Sheng, C.-C. Chen, J.-C. Zhao, *J. Am. Chem. Soc.* **2021**, *143*, 2984-2993.

[30] Y. X. Bian, M. Kim, T. Li, A. Asthagiri, J. F. Weaver, *J. Am. Chem. Soc.* **2018**, *140*, 2665-2672.

10.1002/anie.202407791

Entry for the Table of Contents

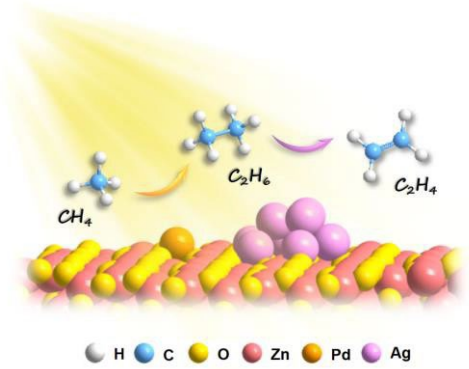

We present a bimetallic design of Ag nanoparticles (NPs) and Pd single atoms (SAs) on ZnO for the cascade photocatalytic CH_4 conversion toward C_2H_4 with the highest production rate compared with previous works. The synergistic effect of Ag NPs and Pd SAs lowers the overall energy barrier of the activation process of both CH_4 and the resulting C_2H_6, constituting a truly synergistic catalytic system to facilitate the C_2H_4 generation.